Quasimonoenergetic electron beam and brilliant gamma-ray radiation generated from near critical density plasma due to relativistic resonant phase locking

B. Liu,[1,2,3] R. H. Hu,[1] H. Y. Wang,[1] D. Wu,[1] J. Liu,[2] C. E. Chen,[1] J. Meyer-ter-Vehn,[4] X. Q. Yan,[1,a)] and X. T. He[1,2,b)]
[1]*Key Laboratory of HEDP of the Ministry of Education, CAPT, and State Key Laboratory of Nuclear Physics and Technology, Peking University, Beijing 100871, China*
[2]*Institute of Applied Physics and Computational Mathematics, Beijing 100088, China*
[3]*Institute for Computational and Plasma Physics, Ludwig-Maximilian-Universität, 80333 München, Germany*
[4]*Max-Planck-Institut für Quantenoptik, D-85748 Garching, Germany*

(Received 9 June 2015; accepted 11 August 2015; published online 31 August 2015)

We show that a high current quasi-monoenergetic electron beam and a peaked brilliant gamma-ray beam can be generated by irradiating an ultra-intense laser pulse on uniform near critical density plasma, with a laser spot radius $R_L \sim (\lambda/\pi)\sqrt{2a/n}$, here λ is the laser wave length, a denotes the normalized laser intensity, and n denotes the normalized plasma density. Due to a relativistic resonant phase locking mechanism, high energy oscillating electrons are trapped to ride on the laser electric field, and an unprecedented ultra-fast ultra-brilliant gamma-ray pulse is emitted from the electrons. Both the high energy electrons and gamma-ray photons are emitted in a small polar angle range. It is similar to a conventional wiggler synchrotron, except that the curvature radius of electron orbits in the laboratory coordinate frame measures in microns rather than in meters. © *2015 AIP Publishing LLC*. [http://dx.doi.org/10.1063/1.4929848]

With the rapid development of ultra-intense laser technology, laser driven electron acceleration in plasma has made great achievements. GeV level collimated monoenergetic electron beams are generated from underdense plasma driven by ultra-short relativistic laser pulses.[1–4] One of the most important applications of high energy electron beams is to produce X-ray or gamma-ray pulses. Recently, all-optical controllable high energy photon sources have attracted much attentions.[5–10] By propagating hundreds of MeV electron beams, up to 100 MeV photons are produced via the bremsstrahlung approach.[6] By interacting high energy electrons in laser driven bubble with the driven laser pulse, MeV synchrotron-like photons can be generated.[8] By scattering 500 MeV electron beam with relativistic laser pulse, up to 18 MeV and brightness 10^{21} photons/s/mm^2/mrad^2/0.1% bandwidth have been produced.[10] However, the number of high energy electrons per shot from underdense plasma is usually very small ($<10^{10}$), which limits the photon number and the brightness of the radiation.

By irradiating an ultra-intense laser pulse on a near critical density plasma, high current high energy electrons and photons can be generated.[11–14] In a self-formed plasma channel,[15] after a pre-acceleration process, a great amount of electrons can interact with the driven laser pulse and directly get energy from the laser pulse.[11,16] A broad spectrum X-ray radiation with a large number of photons and very high energy conversion efficiency from the driven laser to the radiation is demonstrated in experiment.[12,13] However, experimental results show that the electron spectrum is thermal-like and the radiation divergence angle is very large, about $\pi/3$ rad,[13] which surely limits the brightness of high energy photons.

In a previous work,[16] we have shown that more electrons can match resonance conditions via a self-matching mechanism during pre-acceleration process when using a circularly polarized (CP) laser pulse. In this paper, we first show that the resonance conditions can be kept throughout the whole acceleration process due to a novel relativistic resonant phase locking mechanism, and predict that both the output electron beam and radiation can exhibit peaked spectra, provided a stable near critical density plasma channel is formed. Due to phase locking, high energy oscillating electrons are trapped to ride on the laser electric field, and emit high energy photons continuously, eventually a stable bunched quasi-monoenergetic electron beam, as well as a collimated, peaked, brilliant gamma-ray beam can be generated.

Now we consider the electron motion driven by a CP laser pulse in a stable self-formed plasma channel. For a linearly polarized (LP) laser pulse, although there exists parametric amplification effect,[17] and there are less electrons caught during the pre-acceleration process, most of the arguments during the acceleration process that follow can be approximately applied to the LP case, by geometrically considering the LP case as a two-dimensional projection of the CP case. The reason for choosing a CP laser is that the model is more simple, and the calculations are somewhat more straightforward. A schematic figure of the distribution of the laser electric field, electrons and emitted radiation is shown in Fig. 1. With the CP laser pulse, electrons tend to rotate transversely in the channel. It is very difficult to analyze the complete complex nonlinear electron dynamics. Here, we focus on the evolution of the relative phase between the

a)X.Yan@pku.edu.cn
b)xthe@iapcm.ac.cn

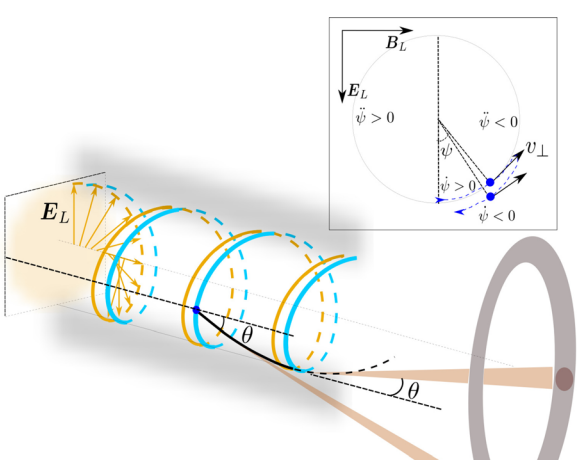

FIG. 1. Schematic figure of the distribution of the laser electric field (a yellow curve), the resonance electrons (a blue curve), the emitted radiation (a gray annular area), and the motion (a black curve) and radiation (two dark red spots on the gray annular area) of a sample electron (a dark blue dot). Inset figure: schematic plot of electron acceleration and motion.

electron rotation and the periodic laser field. Depending on the relative phase ψ, electrons can gain or lose energy. The relative motion is schematically shown in the inset figure. Let $\boldsymbol{\psi}$ denote the relative angle from $\boldsymbol{E}_L$ to $\boldsymbol{r}$, where $\boldsymbol{E}_L$ denotes the electric field of the laser pulse at $\boldsymbol{r}$, and $\boldsymbol{r}$ denotes the distance from the center of the channel to the electron position. The phase evolution of the electron can be illustrated by a simple Hamiltonian system. By ignoring the fast radial oscillation, we can write the equations of the transverse momentum and the energy in normalized form

$$d(\gamma\beta)/d\tau = \kappa a \sin\psi, \tag{1}$$

$$d\gamma/d\tau = \beta a \sin\psi, \tag{2}$$

where $a = eE_L/m_e c\omega_0$, $\tau = \omega_0 t$, $\beta = v_\perp/c$, γ is the Lorentz factor, $\kappa = 1 - v_z/v_{ph}$, v_z is the longitudinal velocity, v_{ph} denotes the phase velocity of the laser pulse, e, m_e is the charge and mass of electron, ϵ_0 is the vacuum permittivity, ω_0, c is the laser frequency and laser velocity in vacuum, respectively. The relative phase can be separated into two parts, an acceleration phase, $0 < \psi < \pi$, and a deceleration phase, $-\pi < \psi < 0$. Due to the self-matching mechanism, only at $\psi \sim 0$, electrons can be resonant with the laser pulse and get energy to escape the trapping of the axial magnetic field;[16] thus, we consider that a relativistic electron is initially injected into the acceleration phase from $\psi \sim 0$, $\gamma \geq 1$. The derivation of the relative phase is equal to the difference between the betatron frequency ω_B and the laser frequency in the electron frame $\omega_L = \kappa\omega_0$. The betatron frequency can be estimated as[18] $\omega_B = \omega_p/\sqrt{\gamma}$, where ω_p is the plasma frequency. Then, we have

$$d\psi/d\tau = \chi/\sqrt{\gamma} - \kappa, \tag{3}$$

where $\chi = \omega_p/\omega_0$. Here, by considering the electron betatron frequency, the confinement effect of the self-generated field in the channel is included. At first, the electron rotates very fast, i.e., $\dot{\psi} > 0$. Due to the electron relativistic effect, the betatron frequency decreases with energy increasing, i.e., $\ddot{\psi} < 0$. If the transverse rotation velocity is not very large, so that $\dot{\psi}$ reaches 0 before ψ reaches π, then the phase ψ will decrease, and the electron is caught by the laser electric field, as illustrated by an arrowed dashed blue line in the inset figure. When the electron passes the point $\psi = 0$ again, it has the maximum energy. Since the relative phase evolves very slow compared with the laser frequency, the phase of the electron motion and the phase of the laser field are locked for a prolonged intervals. The phase locking is caused due to the combination of the resonance and the electron relativistic effect. It is noticed that the high energy transversely oscillating electrons have a relative phase $\psi \sim 0$. It is different with the case of electrons simply driven by a laser pulse.

For relativistic electrons, i.e., $\gamma \gg 1$, we have $\beta \to \sqrt{\kappa} \to$ const. Then, from Eqs. (2) and (3), we can get a closed dynamical system with variables ψ and γ. The phase space spanned by the canonical variables γ and ψ is conserved, and a Hamiltonian can be derived

$$\mathcal{H} = 2\chi\sqrt{\gamma} - \kappa\gamma + \beta a \cos\psi. \tag{4}$$

The phase portrait is shown in Fig. 2(a) by black dotted lines. There are two fixed points: a stable one is at $\psi = 0$ and an unstable one is at $\psi = \pm\pi$. There is a separatrix between the oscillating region and the running away region, denoted by a red dashed line. It is similar to the phase stability motion in both conventional accelerators[19,20] and inverse free electron laser accelerators.[21] The relative phase ψ varies very slow compared with the laser phase. This means, in the laboratory frame of reference, the electron spends too much time in the acceleration phase. Above analysis is valid for all resonance electrons at different laser phase. Thus, high energy electrons are trapped to ride on the laser electric field and exhibit helical distribution. Finally, a high current quasi-monoenergetic electron beam peaked at several hundreds of MeV, and an ultra-short collimated brilliant gamma-ray pulse peaked at multi-MeV are emitted, along a fixed emission angle θ, with a small divergency.

In order to form long stable channel, near critical density plasma is required. In dilute plasma, since $\omega_p \ll \omega_0$, the length of the plasma cavity is limited to the plasma wavelength. In near critical density plasma, although $\omega_p \sim \omega_0$, an ultraintense laser pulse ($a \gg n$) can propagate in the plasma in relativistic transparent regime, and the length of the plasma channel can be far beyond the plasma wavelength. In the relativistic transparent regime, from the dispersion relationship $v_{ph}^2 = c^2(1 - \omega_p^2/\omega_0^2)$ and $\omega_p^2/\omega_0^2 = n\sqrt{1+a^2}$, we have $v_{ph} = c(1 - n/\sqrt{1+a^2})^{-1/2}$, here $n = n_e/n_c$, n_e denotes the plasma density, and $n_c = m_e\omega_0^2\epsilon_0/e^2$ is the critical plasma density. At the limit of $a \gg 1$ and $v_z \to c$, we find $\kappa = 1 - \sqrt{1 - n/a} = n/2a$. Then, we can get the transverse radius of motion of trapped electrons, $R_t = \beta c/\omega_\beta = \lambda/2\pi\sqrt{\kappa} = (\lambda/2\pi)\sqrt{2a/n}$, here $\lambda = 2\pi c/\omega_0$ is the laser wavelength in vacuum. In order to form a stable plasma channel, it is required that the laser spot radius R_L is large enough to contain the transverse oscillation of high energy

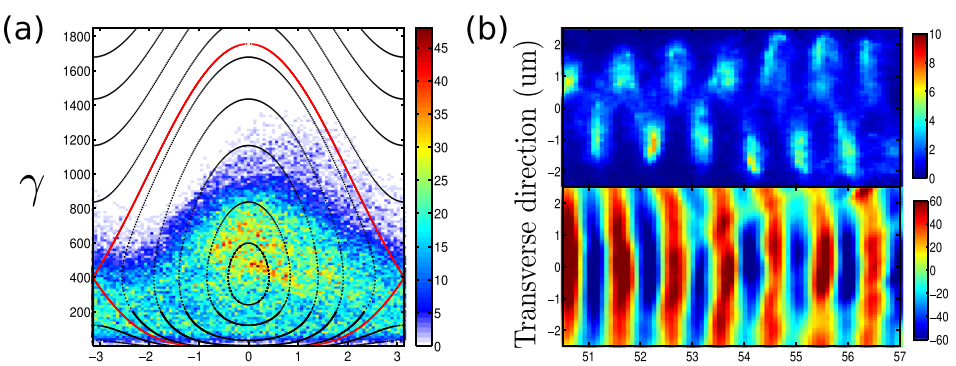

FIG. 2. (a) Snapshot of electrons (phasespace density in arbitrary unit) and phase portrait (solid lines) of the Hamiltonian of Eq. (4) in the phase space spanned by ψ and γ and (b) snapshot distribution of electron density n_e/n_c (upper panel) and transverse electric field $eE_y/m_e c\omega_0$ (lower panel) in y–z section at simulation time 230 fs. The phase portrait in (a) is plotted by assuming $\kappa = 0.05$ and $\chi = 1$.

electrons and not too large to stimulate strong self-focusing. Then, we rederived the condition for stable plasma channel formation in near critical density plasma

$$R_L \sim 2R_t = (\lambda/\pi)\sqrt{2a/n}. \tag{5}$$

In order to show the details of the gamma-ray radiation, we have run three-dimensional (3D) particle in cell (PIC) simulations. A CP laser pulse with laser intensity $10^{22}\,\mathrm{W/cm^2}$, central wavelength $\lambda = 1\,\mu\mathrm{m}$, wave period $T_0 = \lambda_0/c$, duration time $20T_0$, spot radius $R_L = 7\ \mu\mathrm{m}$, and a transverse (X,Y) Gaussian envelope with $a_r = a_0 \exp(-(x^2+y^2)/4R_L^2)$ is normally incident on the left boundary ($z = 0$) of a $100 \times 50 \times 50\,\mu\mathrm{m}^3$ simulation box with a grid of $1200 \times 600 \times 600$ cells. Since $R_t = R_L/2$, we have $a \sim a_0 = 60$ for resonance electrons. In this condition, the nonlinear QED effect can be neglected,[22,23] the motion of electrons can be calculated from the Lorentz-Abraham-Dirac (LAD) equation, and the electromagnetic radiation is dominated by the synchrotron-like radiation regime. We extend a fully relativistic 3D PIC code (KLAP)[24] to consistently include the radiation process and the recoil force by using the method outlined in Ref. 25. A near-critical density plasma target consisting of electrons and protons is located in $6\,\mu\mathrm{m} < z < 71\,\mu\mathrm{m}$. In the laser propagation direction, the plasma density rises linearly from 0 to $n_0 = 1.115 \times 10^{21}/\mathrm{cm}^3$ over a distance of 5 μm and then remains constant. In the radial direction, the density is uniform. The number of superparticles used in the simulation is about 2.2×10^9 for each species (eight particles per cell for each species correspond to n_0). The initial temperature of electrons and ions are T_e of 150 keV and $T_i = 10\,\mathrm{eV}$, respectively.

When irradiating the ultra-intense laser pulse on the plasma, after an unstable filamentary stage, electrons are expelled and an ion channel is self-formed. With the resonance acceleration gradually being dominant, a great amount of high energy electrons are accelerated and propagate along forward direction. A snapshot of the distribution of electrons in the ψ–γ phase space at 230 fs is illustrated in Fig. 2(a). It is shown that most of the high energy electrons are located around the fixed point at $\psi = 0$. A snapshot of the distribution of electron density and the laser electric field at $t = 230$ fs is shown in Fig. 2(b). It is verified that most of the electrons in the channel are phase synchronized with the laser electric field.

The final angular-spectral distribution and spectrum of electrons and radiation are shown in Fig. 3. The results are calculated by accumulating the forward electrons and photons, respectively, at $z = 90\ \mu\mathrm{m}$ over the entire simulation time. Both the high energy electrons and the high energy radiation are mainly located around an emission angle $\theta \sim \pi/12$ rad, with a full divergence angle about $\pi/18$ rad. The angular-spectral distribution and the corresponding energy spectrum of electrons at the emission angle is shown in Fig. 3(a). The upper panel shows that electrons are separated into two parts, high energy part distributed within an emission angle $\pi/18 < \theta < \pi/9$, and low energy part (<200 MeV) spread over all polar angle. The lower panel shows that more than 10^{11} high energy electrons exhibit a quasi-monoenergetic spectrum, peaked at about 400 MeV. It is very different from the thermal spectrum shown in previous works on laser plasma interaction with similar parameters.[11–13] The photon number distribution is shown in Fig. 3(b). In the upper panel, it is shown that most of the high energy photons are distributed within the emission angle. In the lower panel, the photon number exhibits a broad spectrum, similar to the conventional synchrotron wiggler, but covers higher energy range, from keV to 50 MeV, peaked at about 3 MeV. The number of photons with energy greater than MeV is about 10^{12}. The corresponding radiation energy is about 3 J, which is about 2% of the incident laser energy. The duration time of the gamma-ray pulse is close to the length of the electron beam, which is about 20 fs. The radius of the radiation source is about 1 μm. From this, we can get the brightness of the gamma-ray emission in the order of 10^{24} photons/s/mm^2/mrad^2/0.1% bandwidth. By using a LP laser pulse with the same laser energy, a weaker radiation with similar spectrum profile is emitted, as shown by a blue dashed line in the lower panel of Fig. 3(b). Although the number of accelerated electrons in LP case is less than that in CP case, since the radiation is emitted during the acceleration process, the superiority of CP laser is not as strong as that in the case of extreme power laser collision.[27]

For a laser pulse with a smaller spot radius, $R_L \le R_t$, resonance electron cannot be contained in the laser area. For a greater spot radius, $R_L > 3R_t$, the plasma channel is unstable due to the strong laser self-focusing effect. For either of the two cases, it is very difficult to realize self-synchronization between the electron motion and the laser electric field, there is no monoenergetic electron beam, and the radiation is

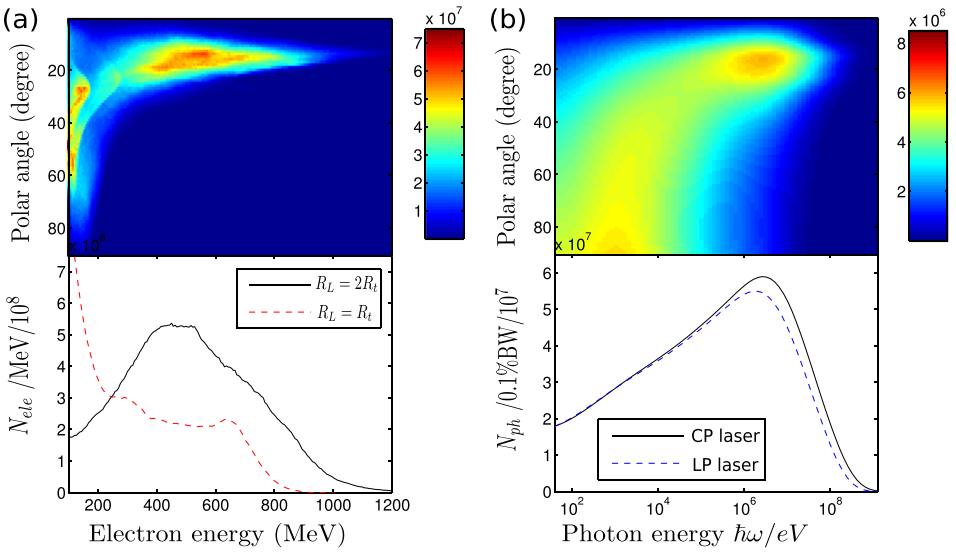

FIG. 3. Simulation results. (a) Upper: final electron angular-spectral distribution (electron number N_{ele} per MeV per mrad^2). Lower: the corresponding electron spectrum (black solid line) and that with a smaller spot size (red dashed line) within emission angle $\pi/18 < \theta < \pi/9$. (b) Upper: final angular-spectral distribution of radiation (photon number N_{ph} per 0.1% bandwidth (BW) per mrad^2). Lower: the corresponding spectrum of photon number (black solid line) and that in the case of a LP laser pulse with the same laser energy (blue dashed line) within emission angle $\pi/18 < \theta < \pi/9$.

weakened. As an example, the final electron spectrum for $R_L = R_t = 3.5$ μm is thermal-like, as shown in the lower panel of Fig. 3(a) by a red dashed line.

The advantages of this radiation regime can be more obvious when the laser intensity is higher. Currently achievable laser intensity is up to 10^{22} W/cm^2.[26] Higher intensity laser can produce brighter radiation. Especially, when the radiation reaction is important for the betatron oscillation electrons, the maximum energy gained by a single electron will be suppressed due to the radiation reaction; however, the number of high energy electrons will increase, with the laser intensity increases. It is noticed that the radiation mechanism we discussed here is different from that discussed in many works in radiation reaction dominant conditions. Our discussion can be extended to lower laser intensity condition, in which lower energy electron beam and radiation can be generated, provided Eq. (5) is satisfied. Furthermore, in many of those works, e.g., in Ref. 28, the radiation emitted mainly due to electron quiver motion. However, in our case, most of the radiation energy is emitted by high energy phase locking electrons. The phase locking mechanism depends on a stable plasma channel, which can be produced in the relativistic self-transparent regime, by irradiating a focused ultra-intense laser pulse on a uniform near critical density plasma. Strong X-ray radiation from electrons performing direct laser radiation in a cavitated channel has been measured with linear polarization laser pulse. Recently, various techniques have been demonstrated to produce near-critical-density plasma targets, including cluster-gas targets,[29] foam,[30] nanotube,[31] and diamond-like carbon targets,[32] indicating that experiments for gamma-ray radiation from near critical dense targets become feasible.

We have investigated high current quasi-monoenergetic and peaked ultra-brilliant gamma-ray generation by propagating an ultra-intense CP laser pulse in a near critical density plasma target. Our proposed emission regime is promising to build compact, brilliant, and adjustable gamma-ray pulse sources, which may change the gamma-ray applications in many areas, including material detection, radiography, medical treatment, high energy physics, etc.

This work was supported by the National Basic Research Program of China (Grant No. 2013CBA01502), National Natural Science Foundation of China (Grant Nos. 11025523, 10935002, 10835003, J1103206, 11205010, and 11305013), and National Grand Instrument Project (2012YQ030142).

[1]A. Pukhov and J. Meyer-ter-Vehn, Appl. Phys. B: Lasers Opt. **74**, 355–361 (2002).
[2]S. P. D. Mangles, C. D. Murphy, Z. Najmudin, A. G. R. Thomas, J. L. Collier, A. E. Dangor, E. J. Divall, P. S. Foster, J. G. Gallacher, C. J. Hooker, D. A. Jaroszynski, A. J. Langley, W. B. Mori, P. A. Norreys, F. S. Tsung, R. Viskup, B. R. Walton, and K. Krushelnick, Nature **431**, 535 (2004); C. G. R. Geddes, C. Toth, J. van Tilborg, E. Esarey, C. B. Schroeder, D. Bruhwiler, C. Nieter, J. Cary, and W. P. Leemans, Nature **431**, 538 (2004); J. Faure, Y. Glinec, A. Pukhov, S. Kiselev, S. Gordienko, E. Lefebvre, J.-P. Rousseau, F. Burgy, and V. Malka, Nature **431**, 541 (2004).
[3]S. Kneip, S. R. Nagel, S. F. Martins, S. P. D. Mangles, C. Bellei, O. Chekhlov, R. J. Clarke, N. Delerue, E. J. Divall, G. Doucas, K. Ertel, F. Fiuza, R. Fonseca, P. Foster, S. J. Hawkes, C. J. Hooker, K. Krushelnick, W. B. Mori, C. A. J. Palmer, K. T. Phuoc, P. P. Rajeev, J. Schreiber, M. J. V. Streeter, D. Urner, J. Vieira, L. O. Silva, and Z. Najmudin, Phys. Rev. Lett. **103**, 035002 (2009).
[4]W. P. Leemans, A. J. Gonsalves, H.-S. Mao, K. Nakamura, C. Benedetti, C. B. Schroeder, C. Tóth, J. Daniels, D. E. Mittelberger, S. S. Bulanov, J.-L. Vay, C. G. R. Geddes, and E. Esarey, Phys. Rev. Lett. **113**, 245002 (2014).
[5]R. D. Edwards, M. A. Sinclair, T. J. Goldsack, K. Krushelnick, F. N. Beg, E. L. Clark, A. E. Dangor, Z. Najmudin, M. Tatarakis, B. Walton, M. Zepf, K. W. D. Ledingham, I. Spencer, P. A. Norreys, R. J. Clarke, R. Kodama, Y. Toyama, and M. Tampo, Appl. Phys. Lett. **80**, 2129 (2002).
[6]Y. Glinec, J. Faure, L. L. Dain, S. Darbon, T. Hosokai, J. J. Santos, E. Lefebvre, J. P. Rousseau, F. Burgy, B. Mercier, and V. Malka, Phys. Rev. Lett. **94**, 025003 (2005).
[7]S. Cipiccia, S. M. Wiggins, R. P. Shanks, M. R. Islam, G. Vieux, R. C. Issac, E. Brunetti, B. Ersfeld, G. H. Welsh, M. P. Anania, D. Maneuski, N. R. C. Lemos, R. A. Bendoyro, P. P. Rajeev, P. Foster, N. Bourgeois, T. P. A. Ibbotson, P. A. Walker, V. O. Shea, J. M. Dias, and D. A. Jaroszynski, J. Appl. Phys. **111**, 063302 (2012).
[8]S. Cipiccia, M. R. Islam, B. Ersfeld, R. P. Shanks, E. Brunetti, G. Vieux, X. Yang, R. C. Issac, S. M. Wiggins, G. H. Welsh, M.-P. Anania, D. Maneuski, R. Montgomery, G. Smith, M. Hoek, D. J. Hamilton, N. R. C. Lemos, D. Symes, P. P. Rajeev, V. O. Shea, J. M. Dias, and D. A. Jaroszynski, Nat. Phys. **7**, 867–871 (2011).
[9]S. Chen, N. D. Powers, I. Ghebregziabher, C. M. Maharjan, C. Liu, G. Golovin, S. Banerjee, J. Zhang, N. Cunningham, A. Moorti, S. Clarke, S. Pozzi, and D. P. Umstadter, Phys. Rev. Lett. **110**, 155003 (2013); N. D. Powers, I. Ghebregziabher, G. Golovin, C. Liu, S. Chen, S. Banerjee, J. Zhang, and D. P. Umstadter, Nat. Photon **8**, 28–31 (2014); C. Liu, G.

Golovin, S. Chen, J. Zhang, B. Zhao, D. Haden, S. Banerjee, J. Silano, H. Karwowski, and D. Umstadter, Opt. Lett. **39**, 4132–4135 (2014).
[10]G. Sarri, D. J. Corvan, W. Schumaker, J. M. Cole, A. Di Piazza, H. Ahmed, C. Harvey, C. H. Keitel, K. Krushelnick, S. P. D. Mangles, Z. Najmudin, D. Symes, A. G. R. Thomas, M. Yeung, Z. Zhao, and M. Zepf, Phys. Rev. Lett. **113**, 224801 (2014).
[11]A. Pukhov, Z.-M. Sheng, and J. Meyer-ter-Vehn, Phys. Plasmas **6**, 2847 (1999).
[12]C. Gahn, G. D. Tsakiris, A. Pukhov, J. Meyer-ter-Vehn, G. Pretzler, P. Thirolf, D. Habs, and K. J. Witte, Phys. Rev. Lett. **83**, 4772–4775 (1999).
[13]S. Kneip, S. R. Nagel, C. Bellei, N. Bourgeois, A. E. Dangor, A. Gopal, R. Heathcote, S. P. D. Mangles, J. R. Marquès, A. Maksimchuk, P. M. Nilson, K. T. Phuoc, S. Reed, M. Tzoufras, F. S. Tsung, L. Willingale, W. B. Mori, A. Rousse, K. Krushelnick, and Z. Najmudin, Phys. Rev. Lett. **100**, 105006 (2008).
[14]H. Y. Wang, B. Liu, X. Q. Yan, and M. Zepf, Phys. Plasmas **22**, 033102 (2015).
[15]A. Pukhov and J. Meyer-ter-Vehn, Phys. Rev. Lett. **76**, 3975 (1996).
[16]B. Liu, H. Y. Wang, J. Liu, L. B. Fu, Y. J. Xu, X. Q. Yan, and X. T. He, Phys. Rev. Lett. **110**, 045002 (2013).
[17]A. V. Arefiev, B. N. Breizman, M. Schollmeier, and V. N. Khudik, Phys. Rev. Lett. **108**, 145004 (2012).
[18]K. T. Phuoc, F. Burgy, J.-P. Rousseau, V. Malka, A. Rousse, R. Shah, D. Umstadter, A. Pukhov, and S. Kiselev, Phys. Plasmas **12**, 023101 (2005).
[19]V. I. Veksler, Comptes Rendus (Dokaldy) de l'Academie Sciences de l'URSS **43**(8), 329–331 (1944).
[20]E. M. McMillan, Phys. Rev. **68**, 143 (1945).
[21]E. D. Courant, C. Pellegrini, and W. Zakowicz, Phys. Rev. A **32**, 2813 (1985).
[22]C. Bula, K. T. McDonald, E. J. Prebys, C. Bamber, S. Boege, T. Kotseroglou, A. C. Melissinos, D. D. Meyerhofer, W. Ragg, D. L. Burke, R. C. Field, G. Horton-Smith, A. C. Odian, J. E. Spencer, D. Walz, S. C. Berridge, W. M. Bugg, K. Shmakov, and A. W. Weidemann, Phys. Rev. Lett. **76**, 3116–3119 (1996).
[23]A. R. Bell and J. G. Kirk, Phys. Rev. Lett. **101**, 200403 (2008).
[24]X. Q. Yan, C. Lin, Z. M. Sheng, Z. Y. Guo, B. C. Liu, Y. R. Lu, J. X. Fang, and J. E. Chen, Phys. Rev. Lett. **100**, 135003 (2008); Z.-M. Sheng, K. Mima, J. Zhang, and H. Sanuki, Phys. Rev. Lett. **94**, 095003 (2005); M. Chen, Z. M. Sheng, J. Zheng, Y. Y. Ma, and J. Zhang, Chin. J. Comput. Phys. **25**, 43 (2008).
[25]I. V. Sokolov, N. M. Naumova, J. A. Nees, G. A. Mourou, and V. P. Yanovsky, Phys. Plasmas **16**, 093115 (2009).
[26]S.-W. Bahk, P. Rousseau, T. A. Planchon, V. Chvykov, G. Kalintchenko, A. Maksimchuk, G. A. Mourou, and V. Yanovsky, Opt. Lett. **29**, 2837–2839 (2004).
[27]S. S. Bulanov, T. Zh. Esirkepov, A. G. R. Thomas, J. K. Koga, and S. V. Bulanov, Phys. Rev. Lett. **105**, 220407 (2010); S. V. Bulanov, T. Zh. Esirkepov, M. Kando, J. Koga, K. Kondo, and G. Korn, Plasma Phys. Rep. **41**, 1–51 (2015).
[28]T. Nakamura, J. K. Koga, T. Zh. Esirkepov, M. Kando, G. Korn, and S. V. Bulanov, Phys. Rev. Lett. **108**, 195001 (2012); A. G. R. Thomas, C. P. Ridgers, S. S. Bulanov, B. J. Griffin, and S. P. D. Mangles, Phys. Rev. X **2**, 041004 (2012).
[29]Y. Fukuda, A. Y. Faenov, M. Tampo, T. A. Pikuz, T. Nakamura, M. Kando, Y. Hayashi, A. Yogo, H. Sakaki, T. Kameshima, A. S. Pirozhkov, K. Ogura, M. Mori, T. Z. Esirkepov, J. Koga, A. S. Boldarev, V. A. Gasilov, A. I. Magunov, T. Yamauchi, R. Kodama, P. R. Bolton, Y. Kato, T. Tajima, H. Daido, and S. V. Bulanov, Phys. Rev. Lett. **103**, 165002 (2009).
[30]L. Willingale, S. R. Nagel, A. G. R. Thomas, C. Bellei, R. J. Clarke, A. E. Dangor, R. Heathcote, M. C. Kaluza, C. Kamperidis, S. Kneip, K. Krushelnick, N. Lopes, S. P. D. Mangles, W. Nazarov, P. M. Nilson, and Z. Najmudin, Phys. Rev. Lett. **102**, 125002 (2009).
[31]W. Ma, L. Song, R. Yang, T. Zhang, Y. Zhao, L. Sun, Y. Ren, D. Liu, L. Liu, J. Shen, Z. Zhang, Y. Xiang, W. Zhou, and S. Xie, Nano Lett. **7**, 2307–2311 (2007); J. H. Bin, W. J. Ma, H. Y. Wang, M. J. V. Streeter, C. Kreuzer, D. Kiefer, M. Yeung, S. Cousens, P. S. Foster, B. Dromey, X. Q. Yan, R. Ramis, J. Meyer-ter-Vehn, M. Zepf, and J. Schreiber, Phys. Rev. Lett. **115**, 064801 (2015).
[32]W. J. Ma, J. H. Bin, H. Y. Wang, M. Yeung, C. Kreuzer, M. Streeter, P. S. Foster, S. Cousens, D. Kiefer, B. Dromey, X. Q. Yan, J. Meyer-ter-Vehn, M. Zepf, and J. Schreiber, Phys. Rev. Lett. **113**, 235002 (2014).